

PACS numbers: 42.55.Px; 42.50.Lc; 73.63.Hs
DOI: 10.1070/QE2014v044n04ABEH015309

Equivalent circuit-level model and improvement of terahertz quantum cascade lasers

Wei Zhou, Shaobin Liu, Jie Wu, Xiaoliu Zhang, Wu Tang

Abstract. **An equivalent circuit-level model of terahertz (THz) quantum cascade lasers (QCLs) is developed by using rate equations. This model can be employed to investigate the characteristics of THz QCLs accurately and to improve their design. We use the circuit-level model to analyse a new active structure, which can improve the performance of THz QCLs by means of enhancing carrier injection. The simulation result shows that THz QCLs with the new active structure have a much higher performance compared with conventional THz QCLs. The high-performance THz QCLs are expected to be operated at higher temperatures.**

Keywords: *quantum cascade lasers, circuit-level model, rate equation.*

1. Introduction

The invention of QCLs in 1994 by Faist et al. [1] made it possible to manufacture a powerful and compact solid source of far-IR radiation. Since then, their performances have been continuously improved and nowadays their spectral range is now extending from the mid-IR down to THz.

The THz frequency range is located between microwave and IR regions and ranges from 0.1 THz to 10 THz, respectively. This range is fitted for many applications, such as material characterisation, medical imaging and biological sensing. Due to the novel properties and unique interaction with many materials, THz radiation has become a hot topic of research for the past few years, and is still a going concern [2, 3]. The lack of compact, high power THz sources has limited their practical utilisation. The THz QCLs have emerged as the most powerful semiconductor THz sources in the frequency range of 2–5 THz.

However, the operation of THz QCLs is restricted to low temperature (below 200 K) [4]. In order to improve the operational temperature, many methods are proposed, such as double-phonon resonance [5], which can improve carrier extraction. Nevertheless, such a technique cannot drastically improve performance. However, Sekine and Hosako [6] put forward a new design with a new active structure, which can reduce the threshold pump rate corresponding to the threshold current and increase the slope efficiency, thereby making this design advantageous for the high-temperature operation of THz QCLs. Compared to conventional THz QCLs, QCLs with the new active structure have a higher performance.

Modelling the behaviour of QCLs is an important step toward the prediction of performances of such semiconductor sources. Through modelling, we can investigate the underlying physical processes, study the characteristics of QCLs and find out the critical factors. We can use the model to judge whether this design is effective or not, thus saving both time and money in improving the design.

The approaches of modelling include the nonequilibrium Green's function formalism [7], the Monte Carlo simulation [8] and the model of self-consistent rate equations [9]. The first two approaches are very computationally cumbersome, which makes them unsuitable for optimising the design. In contrast, the model of self-consistent rate equations is precise and fast, which makes it suitable for designing and optimising. Thus, in this paper, we adopt the third approach. We build the model for the conventional and high-performance THz QCLs. Then, we obtain their equivalent circuits and study their characteristics in detail.

2. Modelling of conventional THz QCLs

Analysis of conventional THz QCLs. We consider the active region of conventional THz QCLs as a three-level system [10], which is depicted in Fig. 1 for one stage of the active region.

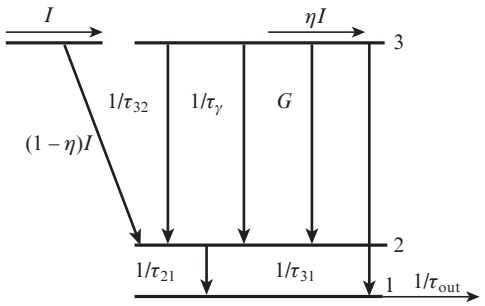

Figure 1. Schematic energy diagram and charge carrier transfer for one stage of the active region of conventional THz QCLs.

The discrete energy levels are labelled 1, 2 and 3. Levels 3, 2, 1 stand for the upper laser state, the lower laser state and the carrier-extraction laser state. The lasing transition is between levels 3 and 2, including spontaneous emission and stimulated emission.

The carriers are injected from the injector region into level 3 [11], by resonant tunnelling. There are also some carriers

Wei Zhou, Shaobin Liu, Jie Wu, Xiaoliu Zhang, Wu Tang State Key Laboratory of Electronic Thin Films and Integrated Devices, University of Electronic Science and Technology of China, Chengdu 610054, China; e-mail: weizhou@uestc.edu.cn, liushaobinbei@126.com

Received 8 September 2013; revision received 4 December 2013
Kvantovaya Elektronika **44** (4) 289–293 (2014)
Submitted in English

scattering from the injector region directly into levels 2 and 1, bypassing level 3. Because the carriers scattering from the injector region directly into the 1st level are few, in this paper we neglect this scattering in order to simplify the calculation. After the radiative transition from level 3 to level 2, the carriers relax into level 1 by emitting longitudinal-optical (LO) phonons and then escaping into the next injector region.

Thus, the rate equations can be written in the form

$$\eta\frac{I}{e}=\frac{\mathrm{d}N_3}{\mathrm{d}t}+\frac{N_3}{\tau_3}+G(N_3-N_2)N_{\mathrm{ph}}, \tag{1}$$

$$(1-\eta)\frac{I}{e}+\frac{N_3}{\tau_{32}}+\frac{N_3}{\tau_\gamma}+G(N_3-N_2)N_{\mathrm{ph}}=\frac{\mathrm{d}N_2}{\mathrm{d}t}+\frac{N_2}{\tau_{21}}, \tag{2}$$

$$\frac{N_3}{\tau_{31}}+\frac{N_2}{\tau_{21}}=\frac{\mathrm{d}N_1}{\mathrm{d}t}+\frac{N_1}{\tau_{\mathrm{out}}}, \tag{3}$$

$$NG(N_3-N_2)N_{\mathrm{ph}}+N\beta\frac{N_3}{\tau_\gamma}=\frac{\mathrm{d}N_{\mathrm{ph}}}{\mathrm{d}t}+\frac{N_{\mathrm{ph}}}{\tau_{\mathrm{ph}}}, \tag{4}$$

where η is the injection efficiency; I is the injection current; N_3, N_2 and N_1 are, respectively, the instantaneous numbers of electrons in 3rd, 2nd and 1st levels; $G=g\Gamma c/(n_{\mathrm{eff}}LW)$ is the rate of induced transitions; g is the differential gain; Γ is the optical confinement; c is the speed of light in vacuum; n_{eff} is the group refractive index; L is the cavity length; W is the cavity width; N_{ph} is the number of photons in cavity; N is the number of QCL stages; τ_{ij} is the nonradiative relaxation time from the ith state to the jth state; τ_γ is the spontaneous relaxation time; $1/\tau_3=1/\tau_{32}+1/\tau_{31}+1/\tau_\gamma$; τ_{out} is the electron escape time; $1/\tau_{\mathrm{out}}$ is the rate of the escape of electrons between two adjacent stages; τ_{ph} is the photon lifetime in the cavity; and β is the coefficient of spontaneous emission.

The relationship between the optical output power P and the number of photon N_{ph} can be written as

$$P=\frac{v_g h\nu}{2L}\ln\left(\frac{1}{r}\right)N_{\mathrm{ph}}, \tag{5}$$

where $v_g=c/n_{\mathrm{eff}}$ is the speed of light in the cavity; h is the Planck constant; ν is the lasing frequency; and r is the reflecting power of the facet.

Circuit-level model. In order to improve the convergence, the quantities N_3, N_2, N_1, N_{ph} and P [system (1)–(4)] are related to the circuit variables V_3, V_2, V_1, V_{ph} and V_{laser}. We assume $N_3=V_3$, $N_2=V_2$, $N_1=V_1$, $N_{\mathrm{ph}}=V_{\mathrm{ph}}$ and $P=V_{\mathrm{laser}}$.

In the upper (3rd) laser-state subcircuit, V_3 is the node voltage,

$$G_{j1}=C_3\frac{\mathrm{d}V_3}{\mathrm{d}t}+\frac{V_3}{R_3}+G_{\mathrm{stim}}. \tag{6}$$

The relationship between the subcircuit elements and the variables of equation (1) is as follows: $G_{j1}=\eta I/e$, $C_3=1$, $R_3=\tau_3$, $G_{\mathrm{stim}}=G(N_3-N_2)N_{\mathrm{ph}}$.

In the lower (2nd) laser-state subcircuit, V_2 is the node voltage,

$$G_{j2}+G_{32}+G_{\mathrm{stim}}=C_2\frac{\mathrm{d}V_2}{\mathrm{d}t}+\frac{V_2}{R_2}, \tag{7}$$

$G_{j2}=(1-\eta)I/e$, $G_{32}=(1/\tau_{32}+1/\tau_\gamma)N_3$, $C_2=1$, $R_2=\tau_{21}$.

In the carrier-extraction (1st) laser-state subcircuit, V_1 is the node voltage,

$$G_{31}+G_{21}+G_{\mathrm{stim}}=C_1\frac{\mathrm{d}V_1}{\mathrm{d}t}+\frac{V_1}{R_1}, \tag{8}$$

$G_{31}=(1/\tau_{31})N_3$, $G_{21}=(1/\tau_{21})N_2$, $C_1=1$, $R_1=\tau_{\mathrm{out}}$.

In the optical subcircuit, V_{ph} is the node voltage and V_{laser} is the output optical power,

$$G_{\mathrm{stim}N}+G_{\mathrm{sp}}=C_{\mathrm{ph}}\frac{\mathrm{d}V_{\mathrm{ph}}}{\mathrm{d}t}+\frac{V_{\mathrm{ph}}}{R_{\mathrm{ph}}}, \tag{9}$$

$$V_{\mathrm{laser}}=\mathrm{G}_{\mathrm{laser}}, \tag{10}$$

$G_{\mathrm{stim}N}=NG_{\mathrm{stim}}$, $G_{\mathrm{sp}}=N\beta N_3/\tau_\gamma$, $C_{\mathrm{ph}}=1$, $R_{\mathrm{ph}}=\tau_{\mathrm{ph}}$,

$$G_{\mathrm{laser}}=\frac{v_g h\nu}{2L}\ln\left(\frac{1}{r}\right)N_{\mathrm{ph}}.$$

A complete circuit-level model is given in Fig. 2 and the symbolic representation of conventional THz QCLs can be described as a three-unit device (Fig. 3).

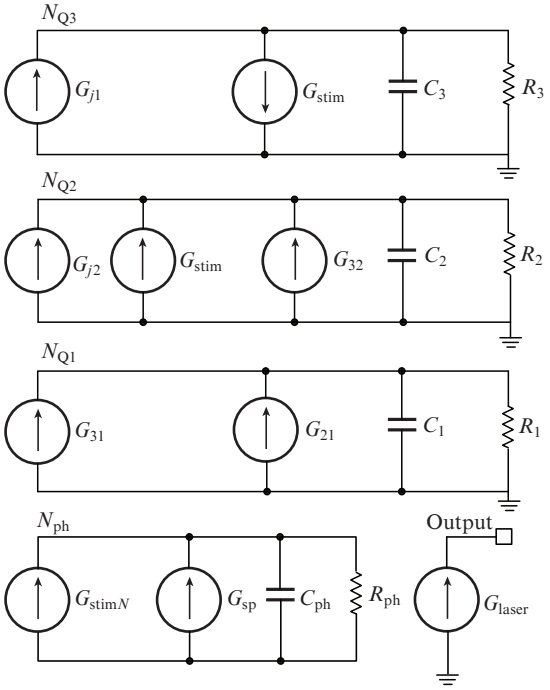

Figure 2. Equivalent circuit of conventional THz QCLs.

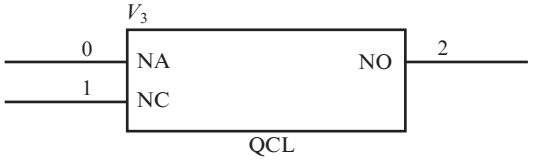

Figure 3. Symbolic representation of conventional THz QCLs: (NA) anode; (NC) cathode; (NO) optical output.

3. Modelling of high-performance THz QCLs

Analysis of THz QCLs. In the introduction we mentioned that the enhancement of carrier extraction cannot largely improve the performance of THz QCLs. Sekine and Hosako [6] pro-

posed a new design with a new active structure, which can enhance carrier injection into the upper laser state. In this new structure, above the upper laser-state, a new laser state is added, which we called the injection state. Carriers are strongly injected by longitudinal optical phonon scattering from the injection state into the upper laser state due to the subpicosecond scattering time in the injection state.

The schematic energy diagram of one stage of the active region of high-performance THz QCLs is given in Fig. 4. Here the 4th level represents the injection state, the 3rd level – the upper laser state, the 2nd level represents the lower laser state and the 1st level stands for the carrier-extraction laser state. The lasing transition is still between levels 3 and 2 and N_4 is the instantaneous numbers of electrons in the injection state.

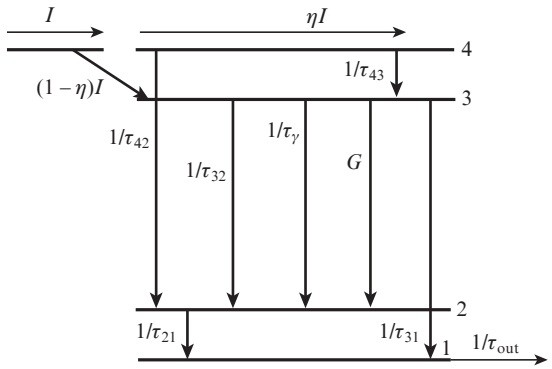

Figure 4. Schematic energy diagram of one stage of the active region of high-performance THz QCLs.

Thus, the equations can be written as

$$\eta\frac{I}{e} = \frac{\mathrm{d}N_4}{\mathrm{d}t} + \frac{N_4}{\tau_{43}} + \frac{N_4}{\tau_{42}}, \tag{11}$$

$$(1-\eta)\frac{I}{e} + \frac{N_4}{\tau_{43}} = \frac{\mathrm{d}N_3}{\mathrm{d}t} + \frac{N_3}{\tau_3} + G(N_3 - N_2)N_{\mathrm{ph}}, \tag{12}$$

$$\frac{N_3}{\tau_{32}} + \frac{N_3}{\tau_\gamma} + \frac{N_4}{\tau_{42}} + G(N_3 - N_2)N_{\mathrm{ph}} = \frac{\mathrm{d}N_2}{\mathrm{d}t} + \frac{N_2}{\tau_{21}}, \tag{13}$$

$$\frac{N_3}{\tau_{31}} + \frac{N_2}{\tau_{21}} = \frac{\mathrm{d}N_1}{\mathrm{d}t} + \frac{N_1}{\tau_{\mathrm{out}}}, \tag{14}$$

$$NG(N_3 - N_2)N_{\mathrm{ph}} + N\beta\frac{N_3}{\tau_\gamma} = \frac{\mathrm{d}N_{\mathrm{ph}}}{\mathrm{d}t} + \frac{N_{\mathrm{ph}}}{\tau_{\mathrm{ph}}}, \tag{15}$$

$$P = \frac{v_g h\nu}{2L}\ln\left(\frac{1}{r}\right)N_{\mathrm{ph}}. \tag{16}$$

Circuit-level model. As in the previous case, the quantities N_4, N_3, N_2, N_1, N_{ph} and P [system (11)–(16)] are related to the circuit variables V_4, V_3, V_2, V_1, V_{ph} and V_{laser}. We assume $V_4 = N_4$, $V_3 = N_3$, $V_2 = N_2$, $V_1 = N_1$, $V_{\mathrm{ph}} = N_{\mathrm{ph}}$, $V_{\mathrm{laser}} = P$.

In injection-state (4th) subcircuit, V_4 is the node voltage,

$$G_{j1} = C_4\frac{\mathrm{d}V_4}{\mathrm{d}t} + \frac{V_4}{R_4}. \tag{17}$$

The relation between the subcircuit elements and the variables of equation (11) is as follows: $G_{j1} = \eta I/e$, $C_4 = 1$, $R_4 = \tau_{43}\tau_{42}/(\tau_{43} + \tau_{42})$.

In the upper (3rd) laser-state subcircuit, V_3 is the node voltage,

$$G_{j2} + G_{43} = C_3\frac{\mathrm{d}V_3}{\mathrm{d}t} + \frac{V_3}{R_3} + G_{\mathrm{stim}}, \tag{18}$$

$G_{j2} = (1-\eta)I/e$, $G_{43} = N_4/\tau_{43}$, $C_3 = 1$, $R_3 = \tau_3$, $G_{\mathrm{stim}} = G(N_3 - N_2)N_{\mathrm{ph}}$.

In the lower (2nd) laser-state subcircuit, V_2 is the node voltage,

$$G_{32} + G_{42} + G_{\mathrm{stim}} = C_2\frac{\mathrm{d}V_2}{\mathrm{d}t} + \frac{V_2}{R_2}, \tag{19}$$

$G_{32} = (1/\tau_{32} + 1/\tau_\gamma)N_3$, $G_{42} = N_4/\tau_{42}$, $C_2 = 1$, $R_2 = \tau_{21}$.

In the carrier-extraction (1st) laser-state subcircuit, V_1 is the node voltage,

$$G_{31} + G_{21} = C_1\frac{\mathrm{d}V_1}{\mathrm{d}t} + \frac{V_1}{R_1}, \tag{20}$$

$G_{31} = (1/\tau_{31})N_3$, $G_{21} = (1/\tau_{21})N_2$, $C_1 = 1$, $R_1 = \tau_{\mathrm{out}}$.

In the optical subcircuit, V_{ph} is the node voltage and V_{laser} is the output optical power,

$$G_{\mathrm{stim}N} + G_{\mathrm{sp}} = C_{\mathrm{ph}}\frac{\mathrm{d}V_{\mathrm{ph}}}{\mathrm{d}t} + \frac{V_{\mathrm{ph}}}{R_{\mathrm{ph}}}, \tag{21}$$

$$V_{\mathrm{laser}} = G_{\mathrm{laser}}, \tag{22}$$

$G_{\mathrm{stim}N} = NG_{\mathrm{stim}}$, $G_{\mathrm{sp}} = N\beta N_3/\tau_\gamma$, $C_{\mathrm{ph}} = 1$, $R_{\mathrm{ph}} = \tau_{\mathrm{ph}}$,

$$G_{\mathrm{laser}} = \frac{v_g h\nu}{2L}\ln\left(\frac{1}{r}\right)N_{\mathrm{ph}}.$$

A complete circuit-level model is shown in Fig. 5. The symbolic representations of both types of QCLs in question are similar (Fig. 3).

4. Results of simulation

In order to fully understand the characteristics of conventional and high-performance THz QCLs, we stimulate them in a PSpice simulator. The device parameters (from [6, 12–14]) are listed below:

Cavity length/μm	3000
Cavity width/μm	.80
Number of QCL stages	.30
Lasing frequency/THz	2.9
τ_{43}/ps	0.5
τ_{42}/ps	100
Group refractive index	.3.27
Differential gain/cm^{-1}	$.5\times10^{-8}$
Optical confinement	.0.27
τ_{32}/ps	2
τ_{31}/ps	2.4
τ_{21}/ps	0.3
Rate of induced transitions/s^{-1}	5.3×10^{4}
Injection efficiency	0.6
Spontaneous emission coefficient	$.2\times10^{-3}$
τ_{out}/ps	0.5
τ_γ/ns	0.5

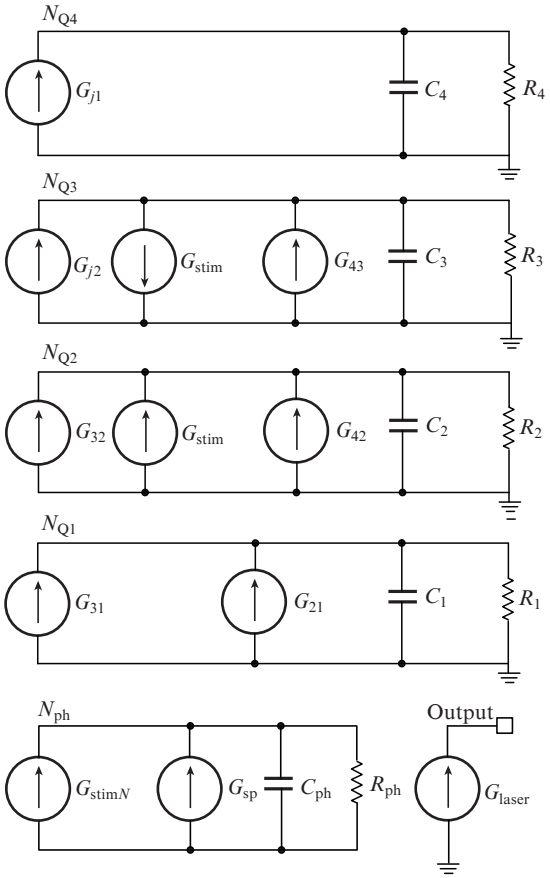

Figure 5. Equivalent circuit of high-performance THz QCLs.

Direct current simulation. The circuit of direct current (DC) simulation used in PSpice is given in Fig. 6a. Figure 7 shows the light–current characteristics of high-performance and conventional THz QCLs. The threshold current of high-performance THz QCLs is 0.75 A, while the threshold current of conventional THz QCLs is 1.65 A. Above the threshold current, the slope efficiency of high-performance THz QCLs is 7.2mW A^{-1}, which is two times that of conventional THz QCLs. The above results suggest that the performance of high-performance THz QCLs is much better.

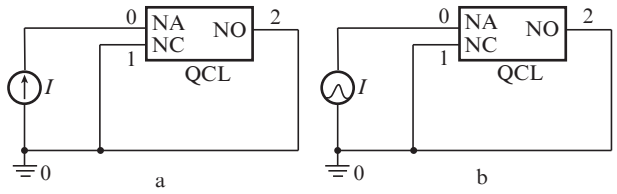

Figure 6. Circuits for (a) simulation at a direct current (0–3 A) and (b) for simulation of transient processes; *I* is the input current pulse.

The effect of the injection efficiency η on the output optical power of QCLs is shown in Fig. 8, which illustrates the light–current characteristics of conventional THz QCLs (at η = 0.9, 0.7 and 0.5) and high-performance THz QCLs. One can see that for conventional THz QCLs, the smaller the η, the larger the threshold current and the smaller the slope efficiency. At the same time, the result of simulation of high-performance THz QCLs shows that at different η the threshold current and the slope efficiency are the same as at $\eta = 0.6$.

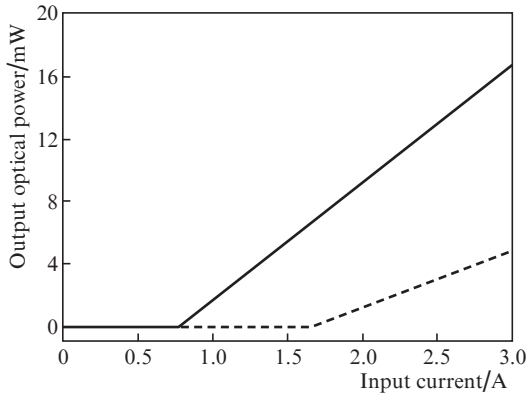

Figure 7. Light–current characteristics of high-performance (solid curve) and conventional (dashed curve) THz QCLs.

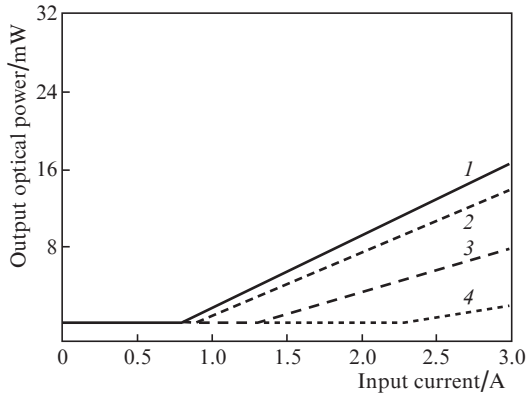

Figure 8. Light–current characteristics of high-performance (*1*) and conventional THz QCLs at η = (*2*) 0.9, (*3*) 0.7 and (*4*) 0.5.

The results of DC simulation are similar to results of Ref. [6] and demonstrate the advantage of high-performance THz QCLs with the new active region over conventional QCLs. The results also confirm that our model is accurate. Because a decrease in η is assumed to correspond to an increase in the temperature of the THz QCLs [6], the high-performance THz QCLs have a higher operating temperature tolerance.

Transient simulation. The circuit of transient simulation used in PSpice is given in Fig. 6b. Figure 9 shows the simulation results. One can see that high-performance THz QCLs have a shorter turn on/off time as well as a maximum output optical power. This means that such THz QCLs can have a quick response and export a larger optical power (Table 1).

5. Conclusions

We have constructed an equivalent circuit-level model of THz QCLs, which can be used to analyse quickly and precisely the characteristics of THz QCLs. Using the circuit-level model, we investigate THz QCLs with a new active structure. The results show that high-performance THz QCLs have a lower threshold current and a larger slope efficiency. Both of them are expected to contribute to improve the operational temperature of the THz QCLs. Besides, the response of THz QCLs can be faster and their output optical power can be

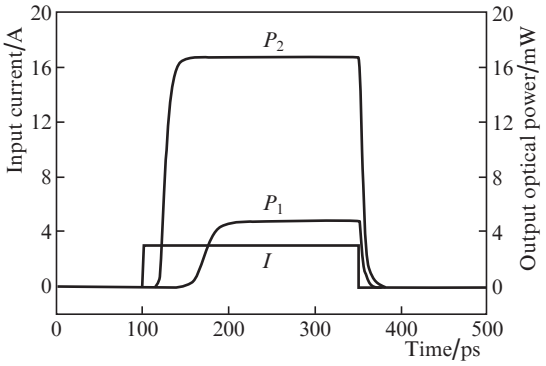

Figure 9. Transient processes in conventional QCLs (P_1) and high-performance QCLs (P_2); I is the input current pulse with amplitude 3 A and duration 250 ps.

Table 1. Comparison of transient characteristics of conventional and high-performance THz QCLs.

Lasers	t_{in}/ps	t_{out}/ps	P_{max}/mW
Conventional THz QCLs	85	39	4.8
High-performance THz QCLs	24	15	16.7

Note: t_{in} is the turn-on time; t_{out} is turn-off time; P_{max} is the maximal output optical power.

improved considerably. All the results will be helpful to make contribution to the development of THz QCLs.

Acknowledgements. This work was supported by the Strategic Priority Research Programme of the Chinese Academy of Sciences (Grant No. XDA01020304), the National Natural Science Foundation of China (Grant Nos 91026005, 11275156, 51071038 and 11305029), Sichuan Province Science Foundation for Youths (Grant No. 2010JQ0002) and State Key Laboratory for Mechanical Behavior of Materials, Xian Jiaotong University (Grant No. 20131309).

References

1. Faist J., Capasso F., Sivco D.L., Sirtori C., Hutchinson A.L., Cho A.Y. *Science*, **264**, 553 (1994).
2. Siegel P.H. *IEEE Trans. Microwave Theory Tech*., **50**, 910 (2002).
3. Saeedkia D., Safavi-Naeini S. *J. Lightwave Technol*., **26**, 2409 (2008).
4. Fathololoumi S., Dupont E., Chan C.W.I., Wasilewski Z.R., Laframboise S.R., Ban D., Matyas A., Jirauschek C., Hu Q., Liu H.C. *Opt. Express*, **20**, 3866 (2012).
5. Williams B.S., Kumar S., Callebaut H., Hu Q., Reno J.L. *Appl. Phys. Lett*., **83**, 2124 (2003).
6. Sekine N., Hosako I. *Phys. Status Solidi C*, **6**, 1428 (2009).
7. Lee S.C., Wacker A. *Phys. Rev. B*, **66**, 245314 (2002).
8. Koehler R., Iotti R.C., Tredicucci A., Rossi F. *Appl. Phys. Lett*., **79**, 3920 (2001).
9. Indjin D., Harrison P., Kelsall R.W., Ikonic Z. *J. Appl. Phys*., **91**, 9019 (2002).
10. Bartalini S., Borri S., Cancio P., Castrillo A., Galli I., Giusfredi G., Mazzotti D., Gianfrani L., Natale P.D. *Phys. Rev. Lett*., **104**, 083904 (2010).
11. Gmachl C., Capasso F., Sivco D.L., Cho A.Y. *Rep. Prog. Phys*., **64**, 1533 (2001).
12. Haldar M.K. *IEEE J. Quantum Electron*., **41**, 1349 (2005).
13. Faist J., Ajili L., Scalari G., Giovannini M., Beck M., Rochat M., Beere H.E., Davies A.G., Linfield E.H., Ritchie D.A. *Philos. Trans. R. Soc. London, Ser. A*, **362**, 215 (2004).
14. Petitjean Y., Destic F., Mollier J.-C., Sirtori C. *IEEE J. Sel. Top. Quantum Electron*., **17**, 22 (2011).